Check for updates

Green Strategy–Based Synthesis of Silver Nanoparticles for Antibacterial Applications

Kenneth Ssekatawa[1,2], Denis K. Byarugaba[1], Charles D. Kato[1], Eddie M. Wampande[1], Francis Ejobi[1], Jesca L. Nakavuma[1], Malik Maaza[3,4], Juliet Sackey[3,4], Edward Nxumalo[5] and John Baptist Kirabira[6]*

[1]College of Veterinary Medicine Animal Resources and Biosecurity, Makerere University, Kampala, Uganda, [2]Department of Biochemistry, Faculty of Biomedical Science, Kampala International University-Western Campus, Kampala, Uganda, [3]UNESCO-UNISA Africa Chair in Nanosciences/Nanotechnology, College of Graduate Studies, University of South Africa (UNISA), Pretoria, South Africa, [4]Nanosciences African Network (NANOAFNET), iThemba LABS-National Research Foundation, Cape Town, South Africa, [5]Institute for Nanotechnology and Water Sustainability, College of Science, Engineering and Technology, University of South Africa, Florida Science Campus, South Africa, [6]Africa Center of Excellence in Materials, Product Development and Nanotechnology, College of Engineering, Design, Art, and Technology, Makerere University, Kampala, Uganda

Antibiotics have been the nucleus of chemotherapy since their discovery and introduction into the healthcare system in the 1940s. They are routinely used to treat bacterial infections and to prevent infections in patients with compromised immune systems and enhancing growth in livestock. However, resistance to last-resort antibiotics used in the treatment of multidrug-resistant infections has been reported worldwide. Therefore, this study aimed to evaluate green synthesized nanomaterials such as silver nanoparticles (AgNPs) as alternatives to antibiotics. UV-vis spectroscopy surface plasmon resonance peaks for AgNPs were obtained between 417 and 475 nm. An X-ray diffraction analysis generated four peaks for both *Prunus africana* extract (PAE) and *Camellia sinensis* extract (CSE) biosynthesized AgNPs positioned at 2θ angles of 38.2°, 44.4°, 64.5°, and 77.4° corresponding to crystal planes (111), (200), (220), and (311), respectively. A dynamic light-scattering analysis registered the mean zeta potential of +6.3 mV and +0.9 mV for PAE and CSE biosynthesized nanoparticles, respectively. Fourier transform infrared spectroscopy spectra exhibited bands corresponding to different organic functional groups confirming the capping of AgNPs by PAE and CSE phytochemicals. Field emission scanning electron microscopy imaging showed that AgNPs were spherical with average size distribution ranging from 10 to 19 nm. Biosynthesized AgNPs exhibited maximum growth inhibitory zones of 21 mm with minimum inhibitory concentration and minimum bactericidal concentration of 125 and 250 μg/ml, respectively, against carbapenem-resistant bacteria.

Keywords: green synthesis, silver nanoparticles, antibiotic resistance, *Prunus africana*, *Camellia sinensis*

INTRODUCTION

The greatest challenge of our generation and generations to come is antimicrobial resistance as different pathogenic bacteria have continuously evolved to become resistant to even the most recently synthesized antibiotics. This scenario has complicated treatment outcomes even to the commonest bacterial infections (Livermore et al., 2011). The U.S. Centers for Disease Control and Prevention (CDC) approximates that antibiotic resistance is accountable for more than 2 million infections and 23,000 deaths each year in the United States, at a direct cost of $20 billion and extra output losses of $35 billion (CDC, 2013). In Europe, an estimated 25,000 deaths are attributable to antibiotic-resistant infections, costing €1.5 billion annually in direct and indirect costs (ECDC, 2018). Even though there is no trustworthy data on economic losses in third world countries, studies in India (Laxminarayan et al., 2015), Tanzania, and Mozambique (Roca et al., 2008; Kayange et al., 2010) pointed out that increased deaths in neonates are attributed to antibiotic-resistant infections. Carbapenems are among the restricted antibiotics that are recommended to treat severe resistant bacterial infections only when all other drugs have failed (Pakyz et al., 2009); however, resistance to carbapenems has been reported worldwide (Ssekatawa et al., 2021a; Ssekatawa et al., 2021b). Thus, the novel, safe, and effective therapeutics for the treatment of carbapenem-resistant infections are urgent.

Repeated attempts to develop alternative approaches such as the use of herbal medicines, fish mucins, and nanotechnology have been made. Of all, the most promising novel therapeutic option in this present scenario is the application of nanoscale materials as antimicrobial agents as they exhibit a very high surface area to volume ratio and exceptional chemical complexities. The nanotechnology field is anticipated to be the gateway in combating both infectious and noninfectious diseases (Morones et al., 2005; Albrecht et al., 2006). For example, organic nanomaterials such as chitosan and lipid nanoparticles and inorganic nanoparticles such as gold have been used as nano-drug delivery systems (Ssekatawa et al., 2020). The coronavirus-19 messenger ribonucleic acid (mRNA) vaccines developed by BioNTech/Pfizer and Moderna are encapsulated, protected, and delivered to the cytosol of the target host cells by the lipid nanoparticle system (Nanomedicine and the, 2020; Machhi et al., 2021; Schoenmaker et al., 2021). Metallic nanoparticles such as silver, copper, zinc, and gold have been reported to possess potent antimicrobial activity (Ssekatawa et al., 2020). Among the metallic nanoparticles, silver nanoparticles (AgNPs), owing to their potent antimicrobial activity against multidrug-resistant pathogens ranging from viruses to prokaryotes to eukaryotes (fungi), have become the center of attention of robust research (Gong et al., 2007). Silver nanoparticles exhibited great antibacterial efficacy against *Vibrio cholera*, *Salmonella typhi Staphylococcus aureus*, *Escherichia coli*, and *Pseudomonas aeruginosa* in previous experiments (Morones et al., 2005; Li et al., 2010). In the 1960s and 70s, a combination of silver nitrate and sulfonamide to form silver sulfadiazine cream with broad-spectrum antimicrobial activity was the first option for topical treatment of burns as its efficacy against *E. coli, S. aureus, Klebsiella sp.,* and *Pseudomonas sp.* fungal and viral infections was laudable (Moyer et al., 1965; Fox and Modak, 1974). However, Nanoscale silver in comparison to non-nanoscale one such as silver nitrate, presents a concurrently high solubility, great chemical reactivity, and formidable broad-spectrum bacterial growth inhibitory activity at very low concentration (Panáček et al., 2006; Bondarenko et al., 2013; Agnihotri et al., 2013; Martinez-Gutierrez et al., 2013). Most importantly, the bactericidal action of nanoparticles is reliant on their physicochemical properties such as size and shape; hence, variability in the mode of action of different forms of nanoparticles may enlighten why resistance to this treatment is yet to be reported (Kvítek et al., 2008; Marková et al., 2012). To date, the bactericidal effect of nanoparticles is yet to be fully clarified. However, it might reside within the capacity of nanoparticles to discharge cations from nano-prearranged surfaces, which irreversibly disorganize bacterial cell walls, inactivate vital proteins, chelate DNA, and lead to the generation of reactive oxygen species (ROS) known to have high microbicidal activity (Rizzello et al., 2013; Durán et al., 2016; Wang et al., 2017; Yin et al., 2020). Additionally, AgNPs have been reported to possess potent anticancer activity. AgNPs exhibited antitumor activity by reducing cell proliferation, promoting intracellular reactive oxygen species, initiating DNA damage, and apoptosis among cancerous tissues (Kumari et al., 2020; Husain et al., 2021a). Thus, AgNPs possess extensive applications in the biomedical field.

Furthermore, the conventional approaches employed to fabricate nanoparticles such as chemical and physical methods have limitations. Physical approaches are not cost-effective because they regularly require extremely expensive equipment, high temperature, and pressure in addition to high energy consumption (Guzmán et al., 2009), hence, making them unpopular in third world countries. Chemo nanoparticle fabrication mainly entails the models of wet chemistry where several chemical reducing agents are exploited to reduce metal salts in solutions (Polavarapu and Liz-Marzán, 2013; Tahir et al., 2013). The main drawbacks faced by chemical methods include the use of costly metal salts in addition to hazardous solvents and reducing agents. Therefore, nanoparticles synthesized by chemical methods exhibit nonselective toxicity to both target bacterial and host cells (Kawata et al., 2009). Additionally, numerous stabilizers are also necessary to thwart the aggregation of nanoparticles to make them physiologically compatible and functional (Castro et al., 2014).

Due to challenges faced by conventional methods used in the fabrication of nanoparticles, researchers have been motivated to invent novel, cost-effective, uncomplicated, eco-friendly biological approaches. Several biological approaches, such as biosynthesis of nanoparticles using bacteria (Husain et al., 2021b), fungi (Singh et al., 2018), and plant extracts (Singh et al., 2018; Verma et al., 2018), have been reported. The most robust and popular of all is the green synthesis of inorganic nanoparticles exploiting green plant extracts with antioxidant activity. At present, possible sources of phytochemicals have been broadly studied in various plant species and plant parts, including leaves, vegetables, fruits, oilseeds, herbs, barks, and roots, as well

FIGURE 1 | Schematic presentation of the probable mechanism of biosynthesis of silver nanoparticles.

as in the extracts of entire plants (Castillo-Henríquez et al., 2020). Moreover, phytochemicals effectively support the green generation of nanoparticles by acting as reductants as well as functionalizing the resultant nanoparticles. Furthermore, the green-based synthesis and functionalization of nanoparticles can be easily executed under normal physiological conditions (Jameel et al., 2020). Without a doubt, due to the double effect of phytomolecules, green-based synthesis meets the criteria of the best approach for preparing nanoparticles for biological applications because the resultant nanoparticles can be instantly applied without any post-synthesis modification (Mie et al., 2014).

Plant extracts possess a wide variety of active biomolecules with antioxidant activity. The biomolecules include phenolic acids, starch, sugars, terpenoids, phytosterols, alkaloids, polyphenol, proteins, enzymes, coenzymes, and ferulic acid esters that play an important part in the bio-reduction, functionalization, and stabilization of nanoparticles (Verma et al., 2019; Akintelu et al., 2020; Verma et al., 2020; Eram et al., 2021). The antioxidant properties of phytochemicals are mainly attributed to the reducing abilities that permit them to operate as reducing agents and singlet oxygen scavengers, therefore reducing metal salts to nanoscale by scavenging electrons from them (Zhang et al., 2020). Thus, the mechanism of green synthesis of silver nanoparticles is due to the constituent phytochemicals donating electrons for the reduction of Ag^+ ions to $Ag^°$ ions, **Figure 1**.
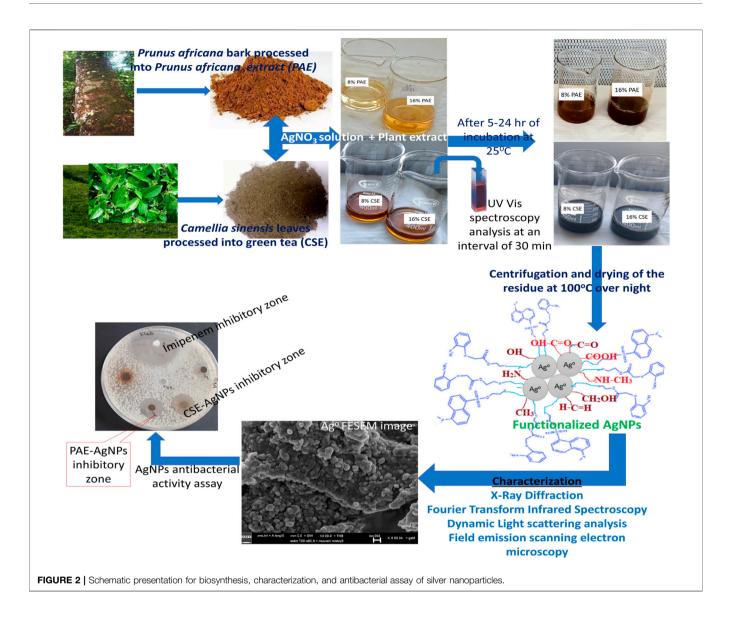
Several reaction parameters determine the size and shape of silver nanoparticles. The reaction parameters include the concentration of silver nitrate, volume/concentration of plant extract, reaction temperature, reaction period, and pH of the reaction mixture. The properties of biosynthesized AgNPs greatly depend on the optimization of the reaction parameters (Usmani et al., 2018). Suitable pH values for AgNPs biosynthesis range from 2 to 14; however, a pH value of 7 has been documented as optimal for the complete reduction of Ag^+ to Ag^0. Furthermore, green synthesis of AgNPs can be attained at different temperatures, though, 25°C (room temperature) has been reported as the optimal temperature for the biosynthesis of small-sized spherical AgNPs (Akintelu et al., 2020). Thus, optimization of the conditions for green synthesis of AgNPs

can be achieved through varying plant extract concentration, pH, reaction time, silver salt concentration, and temperature. Furthermore, the constituent biomolecules in the plant extract influence the properties of nanoparticles and the biomolecules present depend on the plant species. *Prunus africana* and *Camellia sinensis* are medicinal plants with potent antioxidant activity, thus, have the capacity to reduce metal ions to the nanoscale level. This study examined the influence of plant species (*Camellia sinensis* and *Prunus africana*), plant extract concentration, and time of incubation on the properties of biosynthesized AgNPs at constant silver nitrate concentration, pH, and temperature. Additionally, the efficacy of the green synthesized AgNPs against carbapenem-resistant (CR) *E. coli* and *K. pneumoniae* was evaluated. **Figure 2** below is the schematic presentation illustrating biosynthesis, characterization, and biomedical application of AgNPs.

METHODS

Site Description and Source of Materials

This study was carried out at the Pharmacology and Microbiology Laboratories, College of Veterinary Medicine, Animal Resources and Biosecurity, Makerere University; Materials Research Department (MRD), iThemba LABs, Cape Town; and Nanotechnology Unit, Department of Chemical Engineering, University of South Africa, Florida Campus. Processing of plant materials, phytochemical extraction, and green synthesis of AgNPs were conducted from the pharmacology laboratory and MRD, while AgNPs susceptibility assays were executed from the microbiology laboratory. Characterization of nanoparticles was accomplished from MRD and the Nanotechnology Unit. Confirmation of the identity of *Prunus africana* was done from the Department of Botany, Makerere University. Silver nitrate (AgNO₃) was obtained from Sigma-Aldrich, United States, *Camellia sinensis* leaves were purchased from Igara Tea Estates, Bushenyi, while *Prunus africana* bark and leaves were acquired from Maramagambo forest, which covers the southern part of Queen Elizabeth National park located in the Bushenyi district, Uganda.

FIGURE 2 | Schematic presentation for biosynthesis, characterization, and antibacterial assay of silver nanoparticles.

Extraction of Phytochemicals From *Camellia sinensis* and *Prunus africana*

Leaves of *Prunus africana* were analyzed by a botanist at the Department of Botany, Makerere University, to confirm its identity. To obtain *Camellia sinensis* extract (CSE) and *Prunus africana* extract (PAE), plant materials (leaves for CSE and the bark for PAE) were washed, lichens scrapped off, and dried under shade on clean drying tables. The plant materials were then shredded into smaller particles of $1–2 \, cm^2$ using a knife and pulverized into a powdered form using an electric laboratory grinder. Four hundred grams (400 g) of each powdered plant material were dissolved in 1.5 L of sterile distilled de-ionized water in two different extraction bottles and left to stand for 5 days under darkness with daily occasional agitation for homogeneous mixing and extraction. The crude extract was sieved and the filtrate was concentrated by evaporation over steel pans in an oven at 37°C. After evaporation, the dry solid concentrate was scrapped off the pans, and then transferred into clean top screw 50 ml falcon tubes labeled as CSE and PAE and then stored at 4°C.

Synthesis of Silver Nanoparticles Using CSE and PAE

The AgNPs were photosynthesized by adding 1 ml (2%) of CSE concentrate into a round bottom flask containing a 49 ml aqueous solution comprising 85 mg of silver nitrate (0.5 mM). The pH value of the mixture was adjusted to 7. The experiment was replicated to assess the effect of the concentration of plant extract on the yield and characteristics of nanoparticles by using different concentrations (4, 8, and 16%) of CSE. The above procedure was repeated using PAE, **Table 1**. UV-vis absorbance was taken immediately after mixing the plant extract and silver nitrate solution. For further absorbance reading, 5 ml from each sample was dispensed into 15 ml falcon tubes and kept in a

Concentration of *Prunus africana* extract (%)	Volume of plant extract (ml)	Volume of silver nitrate (ml)	Total volume (ml)
2	1	49	50
4	2	48	50
8	4	46	50
16	8	42	50

dark cupboard. The round-bottomed flasks were placed in a dark cabinet and left to stand for 24 h, after which each was equipped with a magnetic stir bar and fixed with a cooling condenser. The reaction mixture was left to stand for 2 h at 85°C, then left to cool down at room temperature followed by centrifuging at 9,000 rpm for 30 min. The sediment obtained was washed numerous times with distilled de-ionized water after which the final precipitate produced was dried at 80°C in an oven for 12 h.

Characterization of Silver Nanoparticles
UV-Vis Spectroscopy
This was achieved using a Cary 5000 UV Vis-NIR Spectrophotometer, Agilent Technologies. The samples were examined by UV-vis spectroscopy operating at a resolution of 1 nm between 190 and 800 nm ranges to analyze the optical property of biosynthesized AgNPs. Absorbance was read at 0 min, 0.5, 1, 2, 3, 4, and 5 h for different concentrations of CSE-AgNO$_3$ solution and at 0 min, 0.5, 1, 2, 3, 4, 6, 8, 10, 12, 24, and 72 h for PAE-AgNO$_3$ mixtures.

X-Ray Diffraction Analysis
About 500 mg of green synthesized AgNPs powder were analyzed with a powder X-ray diffraction (XRD) employing BRUKER AXS diffractometer, D8 Advance (Germany) fitted with Cu-Ka radiation ($\lambda K\alpha_1$ = 1.5406 Å) from 2θ = 0.5°–130°, with increment of $\Delta 2\vartheta$: (0.034°), voltage of 40 kV, current of 40 mA, power of 1.6 kW, and counting time of 0.5 s/step. Generated data was analyzed by OriginPro and resultant peaks two theta values were compared with the standard AgNPs values from the International Center for Diffraction Data (ICDD) database. The average crystal particle size was calculated using Debye–Scherrer's formula given as follows:

$$\phi = \frac{0.9\,\lambda}{\beta \cos \theta},$$

where ø is the crystal particle size, β is full width at half maximum (FWHM), λ is the X-ray wavelength, and θ is the angle subtended in peak.

Fourier Transform Infrared Spectroscopy
Fourier transform infrared spectroscopy with a PerkinElmer Spectrum RX I Fourier transform IR system with a frequency ranging from 400 to 4,000 cm^{-1} and a resolution of 4cm^{-1} and set to perform at least 64 scans per sample was used to investigate the organic functional groups of the plant extracts used in the bio-reduction of silver nitrate to silver nanoparticles as follows: 2 mg of silver nanoparticles and 2 g of potassium bromide (KBr) were desiccated at 200°C under reduced pressure overnight. The dried silver nanoparticles were standardized with 100 mg of KBr and then hard-pressed to form very thin transparent circular pellets. The pellets were screened at 4,000–400 cm^{-1} Wavenumber range. A KBr pellet was used to plot the baseline.

Dynamic Light Scattering and Zeta Potential
Zetasizer Nano ZS, Malvern Panalytical, was used to evaluate the size distribution and zeta potential of silver nanoparticles. The Zetasizer Nano ZS instrument was set to perform 60 times per scan for three times per sample to obtain the mean size distribution of nanoparticles. The DLS technique was employed to analyze the nanoparticle size distribution according to the standard method with some modifications (Chattopadhyay et al., 2013). The concentration of silver nanoparticles of 100 μg/ml was sonicated for 5 min to disaggregate the nanoparticles, and dynamic particle sizes were determined by suspending 0.5 μl of the sonicated nanoparticle suspension in 1 ml of Millipore water in zetasizer cuvette followed by scanning of the nanoparticle suspension by a DLS analyzer. The zeta potential of silver nanoparticles was measured by Zetasizer Nano ZS using the electrophoretic light-scattering technology where 1 mg/ml of nanoparticle suspension was prepared in Milli-Q water in a 900 μl zetasizer disposable cell. The suspension was screened 60 times per scan for three scans to compute the mean zeta potential of silver nanoparticles.

Scanning Electron Microscopy
The size and morphology of the biosynthesized AgNPs were examined by field emission scanning electron microscopy (FESEM), a Carl Zeiss SIGMA model operated at 5 kV. Briefly, a thin film of AgNPs was prepared by spreading 1 mg of each sample on carbon tape followed by coating it with carbon. Surface images were captured at different magnifications. ImageJ software was used to estimate the size distribution of AgNPs.

Silver Nanoparticles Susceptibility Bioassay
Antibacterial activity was assessed by the agar well diffusion method. Carbapenem-resistant *E. coli* ATCC 96522 and *K. pneumoniae* NTCT 9633 obtained from the archives of Microbiology Department CHS, Makerere University, were resuscitated in tryptone soy broth (TSB) and incubated at 37°C for 24 h, then subcultured on MacConkey agar plates at 37°C for overnight. The fresh all night grown cultures were used to prepare a McFarland's turbidity standard equivalent to 0.5 McFarland's units. *E. coli* and *K. pneumonia* lawns were inoculated on two separate sterile Muller Hinton Agar plates with a sterile spreader according to the manufacturer Oxoid, United Kingdom, using the adjusted McFarland's turbidity standard. Three wells labeled as positive control (+ve), negative control (−ve), and AgNPs were bore into the agar plates containing the bacterial lawns using a sterile cork borer. Using a dilution factor of 1:2, AgNPs were diluted using DMSO in bejou bottles and mixed thoroughly, and 50 μl of the resultant diluent was pipetted into the well labeled as AgNPs. An imipenem

disk was used as positive control while distilled water in DMSO was used as a negative control. The setup was left to set for a minimum of 30 min and then incubated at 37°C for 24 h and then checked for antibacterial activity. The zone of clearance for the positive control (+ve), negative control (−ve), and AgNPs were measured and recorded in millimeters. The experiment was replicated thrice to get the average inhibitory zone.

Determination of Minimum Inhibitory Concentration

To assess the MIC, 0.1 g of AgNPs was dissolved in 0.6 ml of sterile distilled de-ionized water in a sterile Eppendorf tube and mixed thoroughly by vortexing to form a solution. Then a setup of eight wells of each extract on a microtiter plate was filled with 0.05 ml of sterile TSB. Two-fold serial dilution was carried out by transfer of 0.05 ml of the AgNP solution from the first well to the eighth well on the microtiter plate containing 0.05 ml of sterile Tryptic soy broth (prepared according to the manufacturer, Oxoid, United Kingdom). 0.5 µl of 0.5 McFarland's turbidity standard prepared by suspension of fresh bacterial culture of *E. coli* and *K. pneumoniae* in separate test tubes were dispensed into their corresponding wells containing diluted AgNPs and incubated aerobically at 37°C for an overnight followed by plating of samples from each well on MHA and left to all night at 37°C under aerobic conditions. MIC was determined from the dilution factor with minimum growth inhibition.

Determination of Minimum Bactericidal Concentration

Minimum bactericidal concentration was determined by further performing a tenfold serial dilution (1/10 and 1/100) for the dilutions that did not show growth under MIC determinations on the MHA plate. The two dilutions were further plated on MHA plates that were incubated at 37°C. After incubation the plates were observed for growth, and MBC was determined from the dilution next to one which has growth.
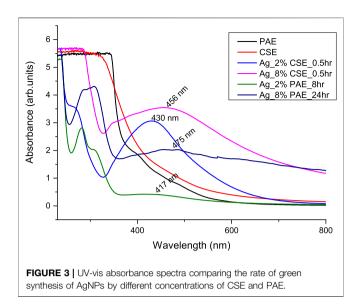
Data Analysis

Data analysis was done using Origin version 2019b. Comparison of the mean zone (diameter in millimeter) of inhibition for CSE-AgNPs and PAE-AgNPs was computed by one-way ANOVA. A p-value of ≤0.05 indicated substantial statistical variance.

RESULTS

Characterization of Green-Synthesized Silver Nanoparticles
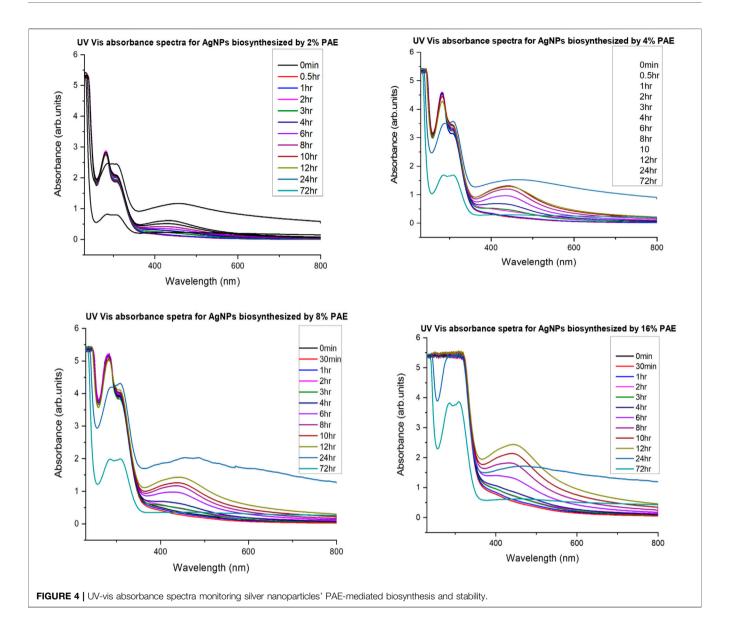
UV-Vis Spectroscopy

UV-vis absorbance spectra of PAE- and CSE-loaded silver nanoparticles solutions were recorded at different time intervals of 0, 0.5, 1, 2, 3, 4, 6, 8, 10, 12, 24, and 72 h and 0, 0.5, 1, 2, 3, 4, and 5 h for PAE and CSE, respectively. The typical surface plasmon resonance (SPR) peaks for PAE- and CSE-generated silver nanoparticles were obtained between 417

FIGURE 3 | UV-vis absorbance spectra comparing the rate of green synthesis of AgNPs by different concentrations of CSE and PAE.

and 475 nm and from 430 to 456 nm, respectively. On the other hand, no SPR peaks were registered for the plant extracts alone throughout the experiment duration; at 0 min, 0.5, 1, 2, and 3 h for all PAE-AgNO₃ treatments; at 0 min for 2, 4, 8, and 16% CSE. An increase in the plant extracts concentration resulted in gradual broadening and shifting of the SPR peaks toward the long wavelength; there was a shift of SPR peaks from 434 nm for 2% PAE to 472 nm for 8% PAE. Likewise, a shift from 430 nm for 2% to 461 nm for 8 and 16% CSE was registered, but more prominently in PAE-photosynthesized nanoparticles. Identical UV-vis absorbance spectra were observed for 8 and 16% CSE-synthesized nanoparticles, **Supplementary Tables S1, S2**; **Figures 3–5**. Furthermore, it is worth noting that the SPR for AgNPs was attained after 30 min with a high absorbance of 3.10 arb. units for CSE, and at 4, 6, and 8 h with very low absorbance for 4, 8, and 2% PAE, respectively. However, 16% PAE had the highest absorbance of 2.40 at 12 h (**Supplementary Tables S1, S2**). Furthermore, SPR bands between 260 and 300 nm were registered (**Figures 4, 5**). PAE- and CSE-mediated photosynthesis of AgNPs was additionally confirmed by a transition from light brown to deep brown for PAE and dark blue for CSE, while silver nitrate solution and plant extracts remained colorless and light brown, respectively, throughout the experiment (**Figure 6**).

X-Ray Diffraction Analysis

An X-ray diffraction analysis generated nine peaks for both PAE- and CSE-biosynthesized AgNPs positioned at 2 θ angles of 27.9°, 32.2°, 38.2°, 44.4°, 46.3°, 54.8°, 57.6°, 64.5°, and 77.4°. However, 38.2°, 44.4°, 64.5°, and 77.4° corresponded to crystal planes (111), (200), (220), and (311), respectively. Peak intensity ranged from 1,004 to 2,824 arb. units and from 313 to 1174 arb. units for CSE- and PAE-mediated synthesized AgNPs. From XRD patterns, the average crystallite size of the silver nanoparticles was computed using the Debye–Scherrer formula. The average crystallite size of PAE and CSE green-synthesized silver nanoparticles ranged from 9 to 32 nm (mean = 17 nm) and from 13 to 29 nm (mean = 21 nm), respectively, **Table 2** and **Figure 7**.

FIGURE 4 | UV-vis absorbance spectra monitoring silver nanoparticles' PAE-mediated biosynthesis and stability.

Fourier Transform Infrared Spectrometry Analysis

FTIR spectra of PAE and CSE exhibited similar bands within wavenumber ranges (cm^{-1}) of 3,650–3,400, 2,960–2,850, 2,349, 2,140–1990, 1,650–1,550, 1,370–1,390, and 800–400. Furthermore, AgNPs biosynthesized by CSE were also capped by unique functional groups with spectra wavenumber ranges (cm^{-1}) of 1,390–1,370 and 1,250–1,020, while PAE green-synthesized AgNPs exhibited distinctive organic functional groups within wavenumber series (cm^{-1}) of 4,000–3,700, 1,560–1,500, 1,440–1,395, 1,310–1,250, and 1,124–1,087, **Table 3** and **Figure 8**.
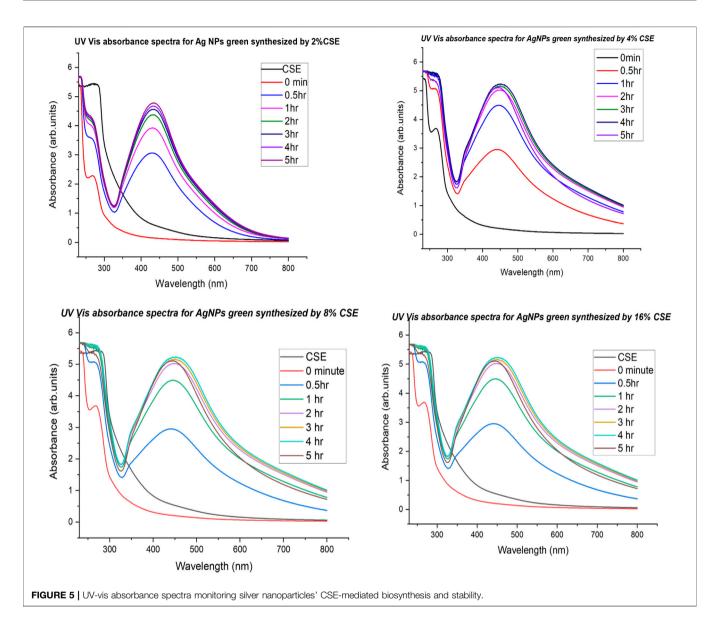
Size Distribution and Zeta Potential

Dynamic light scattering revealed that the size distribution of silver nanoparticles biosynthesized by CSE ranged from 1 to 191 nm with a mean diameter of 51 nm and a mean zeta potential of +0.9 mV. For PAE green-synthesized nanoparticles, size

distribution ranged from 1 to 220 nm with an average diameter of 59 nm and mean zeta potential of +6.3 mV.

Surface Morphology Analysis

A surface morphology analysis by FESEM showed that PAE- and CSE-biosynthesized AgNPs were mainly spherical and aggregated in layers, **Figure 9**. As the concentration of the plant extracts used increased from 2 to 16%, the level of aggregation increased to form large clusters with slimy material on the surface, between individual nanoparticles and aggregates, and is more evident for PAE-photosynthesized nanoparticles. Nanoparticle size computation by ImageJ software from FESEM images showed that the nanoparticles size distribution ranged from approximately 3–98 nm and 4–94 nm for CSE- and PAE-biosynthesized AgNPs, respectively. The average size distribution of nanoparticles increased from 10 to 16 nm and 13–19 nm for CSE-AgNPs

FIGURE 5 | UV-vis absorbance spectra monitoring silver nanoparticles' CSE-mediated biosynthesis and stability.

and PAE-AgNPs, respectively, as the concentration of plant extracts increased from 2 to 16%.
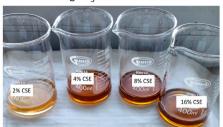
AgNPs Susceptibility Assay

PAE and CSE green-synthesized AgNPs demonstrated potent antibacterial activity with statistically similar growth suppression zones of up to 21 mm for carbapenem-resistant (CR) and -sensitive *E. coli* and *K. pneumoniae*. Furthermore, low MICs and MBCs were registered for the biosynthesized AgNPs, **Tables 4**, **5**.
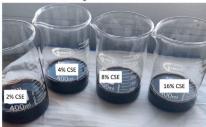
DISCUSSION

The reduction process of silver ions to AgNPs was indicated by a change in color of the reaction mixture from pale brown to dark brown for PAE and dark blue for CSE which was observed

macroscopically. Additionally, AgNP synthesis was confirmed and monitored with UV-vis spectrophotometry. UV-vis spectroscopy is a valuable tool for basic characterization and monitoring of the process of nanoparticle synthesis and stability. This is due to the distinctive optical properties of nanoparticles that enable them to intensely interact with specific wavelengths of UV-visible light spectrum (Sastry et al., 1998; Kelly et al., 2003; Lee and El-Sayed, 2006). Metal surfaces are comparable to plasma, hence possess free electrons in the conductance region and positively charged nuclei. In AgNPs, the forbidden gap between conduction and valence bands is very minute which allows free movement of electrons. This free movement of electrons generates a surface plasmon resonance (SPR) absorption band, owing to the mutual oscillation of AgNPs electrons in resonance with the light wave (Das et al., 2010; Tomaszewska et al., 2013). In this study, the primary characterization and evaluation of CSE- and PAE-mediated AgNPs green synthesis by UV-vis absorbance spectral was successful. UV-vis spectroscopy registered
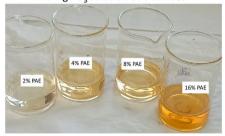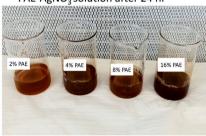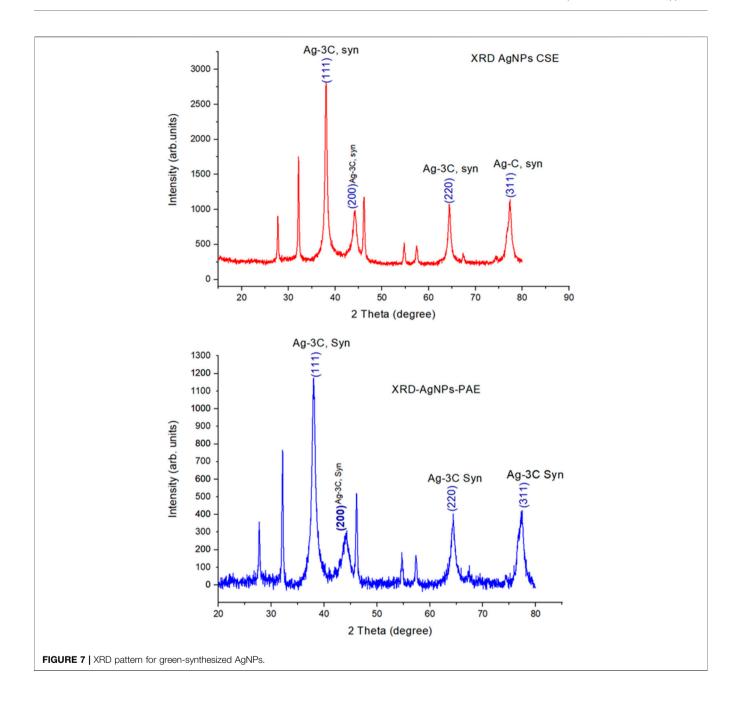
FIGURE 6 | Color transition from light brown at 0 min to dark blue for CSE-AgNO₃ and dark brown for PAE-AgNO₃ suspensions.

TABLE 2 | 2θ values with their corresponding miller's incidences, peak intensity, and average crystal size of CSE and PAE biologically synthesized nanoparticles.

2θ (Degree)	Crystal plane	Ag⁰-CSE intensity (arb. unit)	FWHM (Rad)	Average crystal particle size (nm)	Ag⁰-PAE intensity (arb. units)	FWHM (Rad)	Average crystal particle size (nm)
38.2	(111)	2,824	0.01212	13	1,174	0.02004	9
44.4	(200)	1,004	0.01212	13	312	0.02004	10
64.5	(220)	1,077	0.01212	29	409	0.02004	16
77.4	(311)	1,159	0.01212	27	435	0.02004	32
Mean crystal particle size				**21**			**17**

sharp absorbance SPR band at wavelengths ranging from 436 to 475 nm for PAE and from 430 to 456 nm for CSE, which is a unique optical property for AgNPs (Njagi et al., 2011). Comparable findings were reported in other phytochemical-mediated AgNPs green synthesis studies (Kagithoju et al., 2015; Sahni et al., 2015; Anandalakshmi et al., 2016; Venugopal et al., 2017; Mohamed et al., 2019). The effect of reaction time and plant extract concentration on the green synthesis of nanoparticles was analyzed. The absorption spectra exhibited that the SPR peak rises with increasing extract concentration and time. Therefore, a high concentration of PAE and CSE avail the time-dependent optimum amount of bioactive ingredients required to reduce silver ions to silver nanoparticles. Contrary to this, similar SPR peaks were observed for both concentrations 8 and 16% of CSE used in this study. Furthermore, broadening of the SPR peaks and shift from the blue wavelength toward the long wavelength with increasing concentration of the plant extracts was registered. This is attributed to an increase in size and change in the shape of NPs, a decrease in the NPs interspace, and agglomeration of NPs in colloidal dielectric solutions (Kelly et al., 2003; Lee and El-Sayed, 2006). This specifies that highly concentrated plant extracts, mostly PAE, synthesizes clustered and polydispersed nanoparticles. SPR peaks were registered between 260 and 300 nm, not within the optical range of silver nanoparticles. Shaik et al. (2018), reported similar findings and attributed the SPR bands to absorbance by compounds with benzene and aromatic rings. These bands are associated with π→π* transition (Pongpiacha, 2012; Nasrollahzadeh et al., 2014) and validate the binding of polyphenolics and antioxidant-like compounds with aromatic rings in the plant extracts to the surface of silver nanoparticles (Shaik et al., 2018).

The XRD analysis agreed with UV-vis spectroscopy results. Peaks of AgNPs were displayed in the XRD OriginPro plots ratifying the presence of AgNPs. The XRD array showed four strong peaks located at 2 θ values of 38.0°, 44.3°, 64.5°, and 77.4°. It is worth noting that these values are identical for both PAE and CSE green-synthesized NPs. These values harmonized well with the cubic crystal lattice planes, (111), (200), (220), and (311), respectively, of silver metal using the International Centre for Diffraction Data (ICDD) database (PDF file number 004-0783). However, AgNPs biosynthesized by CSE were of high crystallinity in nature as demonstrated by peaks of higher intensity. Other peaks are corresponding to impurities such as phytochemicals used in the bio-fabrication of AgNPs.

FIGURE 7 | XRD pattern for green-synthesized AgNPs.

FTIR spectroscopy was employed to profile the phytochemicals in PAE and CSE used in bio-reduction of silver ions to nanoscale by identification of the possible organic functional groups capping the AgNPs[1,2] FTIR spectra of PAE and CSE exhibited similar bands within wavenumber ranges (cm^{-1}) of 3,650–3,400, 2,960–2,850, 2,349, 2,140–1990, 1,650–1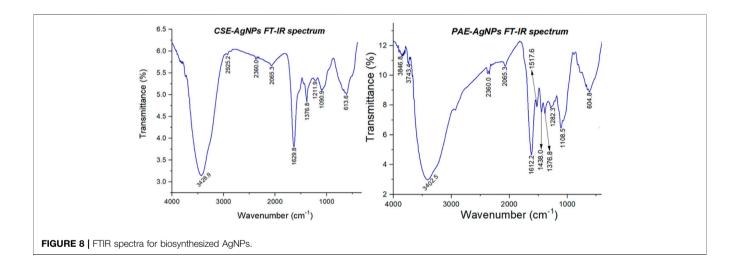,550, 1,390–1,370, and 600–800 assigned to O-H intermolecular stretching bonds found in alcohol or phenols, C-H stretching vibrations in methyl groups alkanes, O=C=O stretching bonds of carbon dioxide, N=C=S stretching bonds of isothiocyanate, N-H bending oscillations of primary amines, C-H bending bonds of gem dimethyl groups in alkanes, and C-Cl stretching bond of halide alkyl correspondingly. However, AgNPs biosynthesized by CSE were also capped by unique functional groups with spectra wavenumber ranges (cm^{-1}) of 1,390–1,370 and 1,250–1,020 associated stretching vibrations of the O-H group in alcohols or phenols and C-N of amine, respectively. Additionally, PAE green-synthesized AgNPs exhibited distinctive organic functional groups within wavenumber series (cm^{-1}) of 4,000–3,700, 1,560–1,500, 1,440–1,395, 1,310–1,250, and

[1]https://www.sigmaaldrich.com/technical-documents/articles/biology/ir-spectrum-table.html, accessed on 30/05/2021.

[2]https://www.thermofisher.com/blog/materials/a-gift-for-you-an-ftir-basic-organic-functional-group-reference-chart/

TABLE 3 | AgNPs-CSE– and AgNPs-PAE–associated organic functional groups as revealed by the FTIR analysis.

Peak intensity	CSE-AgNPs wavenumber (cm^{-1})	PAE-AgNPs wavenumber (cm^{-1})	Functional group wavenumber range (cm^{-1})	Bond	Functional group
Low	—	3846.8	3,700–4,000	O-H	Water
Low	—	3743.4	3,700–4,000	O-H	Water
High	3428.9	3402.5	3,400–3,650	O-H	Alcohol or phenols
Low	2925.2	—	2,960–2,850	C-H	Alkane
Low	2360.0	2360.0	2,349	O=C=O	Carbon dioxide
Low	2065.5	2065.5	2,140–1990	N=C=S	Isothiocyanate
Medium	1629.8	1612.2	1,650–1,550	N-H	Primary amine
Low	—	1517.6	1,560–1,500	N-H	Secondary amide
Low	—	1438.0	1,440–1,395	O-H	Carboxylic acid
Low	1376.8	1376.8	1,370–1,390	C-H	Alkanes
Low	—	1282.3	1,310–1,250	C-O	Aromatic ester
Low	1211.9	—	1,250–1,020	C-N	Amines
Medium	1090.9	—	1,250–1,020	C-N	Amines
Medium	—	1108.5	1,124–1,087	C-O	Secondary alcohol
Medium	613.6	604.8	600–800	C-Cl	Alkyl halide

FIGURE 8 | FTIR spectra for biosynthesized AgNPs.

1,124–1,087 associated with free OH probably due to water, N-H stretching vibrations due to secondary amine, O-H bending vibrations in the carboxylic acid group, and C-O stretching vibrations of secondary alcohol, respectively. Similar to these findings, green tea polyphenols catechins exhibited OH intermolecular bonds linked to methyl functional groups of the different constituent units (Botten et al., 2015).

Owing to its undisputed efficacy in sub-Saharan Africa, PAE has been patented in France as antiprostate cancer and a benign prostate hyperplasia (BPH) agent (Schleich et al., 2006). The confirmed phytochemicals in PAE are: pentacyclic triterpenoids (ursolic and oleanolic acids) which possess terminal OH and COOH groups; phytosterols chiefly β-sitosterol and β-sitostenone with OH, ethyl, and methyl as the main functional groups (Carbin et al., 1990; Bin Sayeed et al., 2016); and Ferulic acid esters (n-tetracosanol and n-docosanol) having COOH, -CHO, -CH2OH, -CH3, and -COOC2H5 as their terminal groups and aromatic rings (Yoshida and Niki, 2003; Kampa et al., 2004). This is in agreement with the findings of this

study as all these functional groups were registered by FTIR. The three classes of phytochemicals possess synergistic effects which thwart biochemical and morphological alterations associated with prostate cancer and BPH. Moreover, these phytochemicals possess potent antioxidant activity (Kikuzaki et al., 2002; Nenadis et al., 2003; Bin Sayeed et al., 2016; Ghante and Jamkhande, 2019). Camellia sinesis processed into green tea contains polyphenols catechins containing OH groups and methyl groups on benzene rings (Botten et al., 2015). They are subdivided into (−)-epigallocatechin-3-gallate (EGCG), (−)-epigallocatechin, (−)-epicatechin-3-gallate, and (−)-epicatechin (EC). Formidable antioxidant activity of catechins most importantly EGCG that affords them to scavenge free radical, hence counteracting oxidative stress has been documented (Forester and Lambert, 2011; Botten et al., 2015; Pasrija and Anandharamakrishnan, 2015; Takahashi et al., 2018). Due to its health benefits, green tea is a beverage to 66% of the world's population (Hajiaghaalipour et al., 2016). This is supported by UV-vis spectroscopy results from this study. CSE
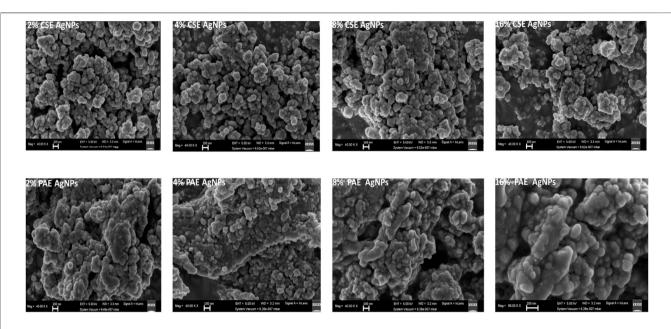
FIGURE 9 | FESEM images of biosynthesized AgNPs. AgNPs represents silver nanoparticles, CSE: *Camellia sinensis* extract, and PAE: *Prunus africana* extract.

synthesized nanoparticles rapidly and at high intensity as compared to PAE.

FESEM images exhibited that AgNPs green synthesized by different concentrations of CSE and PAE were spherical. This is in line with other studies which fabricated AgNPs using plant extracts (Ajitha et al., 2015; Gholami et al., 2018; Hamouda et al., 2019). The nanoparticles were highly aggregated with average size distribution varying from approximately 3–19 nm. Clustering of nanoparticles may be attributed to the interaction of concentrated nanoparticles with the organic components of the plant extracts used in biosynthesis. This is supported by the appearance of a

slime-like substance on the surface and in between nanoparticles especially at high concentrations of plant extracts in FESEM images. The procedure used in the preparation of the film of nanoparticles for FESEM imaging also influences the level of nanoparticle agglomeration. To characterize the particle size and nanostructure using high-resolution scanning electron microscopy (SEM), Chattopadhyay et al. (2013) recommended a method that prepares films with disaggregated nanoparticles. The improved method involves the suspension of nanoparticles in de-ionized water at a concentration of 1 mg/ml followed by sonication to form a homogenous suspension. The homogenous suspension is diluted

TABLE 4 | MIC and MBC values of AgNPs against Carbapenem-resistant *E. coli* and *K. pneumoniae*.

Bacteria type	MIC (mg/ml)		MBC (mg/ml)	
	PAE-AgNPs	CSE-AgNPs	PAE-AgNPs	CSE-AgNPs
Carbapenem resistant *E. coli*	0.125	0.125	0.25	0.25
Carbapenem resistant *K. pneumoniae*	0.25	0.25	0.5	0.5

Notes: MIC: Minimum inhibitory concentration, MBC: Minimum bactericidal concentration, PAE-AgNPs: Prunus africana extract biosynthesized silver nanoparticles, and CSE-AgNPs Camellia sinensis extract biosynthesized silver nanoparticles.

TABLE 5 | Sensitivity tests of AgNPs green-synthesized by PAE and CSE extract showing the inhibitory zone in millimeters.

Organism	Distilled water inhibitory zone (mm)	Imipenem disk inhibitory zone (mm)	PAE-AgNPS inhibitory zone (mm)	CSE-AgNPs inhibitory zone (mm)
Carbapenem-resistant *E. coli*	0	10[B]	18[D]	21[D]
Carbapenem sensitive *E. coli*	0	40[C]	18[D]	21[D]
Carbapenem-resistant *K. pneumoniae*	0	8[B]	20[D]	20[D]
Carbapenem sensitive *K. pneumoniae*	0	40[C]	20[D]	19[D]

Notes: Mean values in each column accompanied by the same letter are not significantly different (p > 0.05) (Tukey Multiple Comparison) and values accompanied by letter (s) which are not similar are significantly different (p < 0.05). PAE-AgNPs: Prunus africana extract biosynthesized silver nanoparticles and CSE-AgNPs: Camellia sinensis extract biosynthesized silver nanoparticles.

using a 1–20 dilution factor and then 1 μl of the diluent is spread onto a carbon tape, dried, gold/carbon-coated, and images taken.

The antimicrobial activity of nanoparticles depends on size and shape distribution. Nanoscale materials with a minute size possess enhanced chemical reactivity, a high diffusion rate, and high penetrative power while those with various form distribution offer different modes of antimicrobial activity (Simon-Deckers et al., 2009; Ssekatawa et al., 2020). PAE- and CSE-mediated biosynthesis attained very small nanoparticles as revealed by FESEM, XRD, and DLS analyses. However, only the spherical form was achieved by this study. Zeta potential estimation using the DLS technique revealed that PAE and CSE green-synthesized AgNPs were positively charged. This promotes an electrostatic interface with the negatively charged bacterial cell walls (Dickson and Koohmaraie, 1989). Thus, minute and positively charged nanoparticles possess enhanced antibacterial activity (Lu et al., 2013).

The antibacterial potential of the green-synthesized AgNPs on human pathogenic CR *E. coli* and *K. pneumoniae* was assessed using the growth inhibitory zone. The NPs demonstrated efficient antibacterial activity with the growth inhibitory zones larger than those achieved in other studies (Raman et al., 2017; Pirtarighat et al., 2019). Furthermore, several antimicrobial bactericide efficacies are dose-dependent (McKenzie, 2011; Verma et al., 2017). However, high concentrations exhibit nonselective cytotoxicity. Therefore, therapeutic agents with very low MIC and MBC are preferable. This study achieved significantly low MIC and MBC of 125/250 and 250/500 μg/ml, respectively, compared to the recommended NP nontoxic dose (100 μg/mg) to mammalian cells and to bactericidal concentration reported by Paul et al. (2018), and way below MICs reported by other studies (Reithofer et al., 2014; Jafari et al., 2018). However, Loo et al. attained extremely low MICs of biosynthesized AgNPs ranging from 3.9 to 7.8 μg/mg (Loo et al., 2018). The susceptibility patterns of both CR and sensitive *E. coli* and *K. pneumoniae* to AgNPs (MIC = 125 μg/ml for *E. coli* and 250 μg/ml for *K. pneumoniae*) were identical which is an indication of no mechanism of resistance to AgNPs in carbapenemase-producing bacteria. Furthermore, compared to CSE-AgNPs, statistically, PAE-AgNPs exhibited smaller zones of bacterial growth inhibition. This may be attributed to 1) bigger size of PAE-AgNPs as small-sized NPs exhibit enhanced antimicrobial activity and 2) higher levels of the slimy PAE materials (proteins and polysaccharides) as revealed by FESEM images that might prevent high rate migration of the nanoparticles within the agar.

CONCLUSION

The evolution of MDR pathogens presents a challenge to healthcare systems and calls for speedy research to design alternative therapeutics such as NPs without compromising the safety of consumers. Therefore, this study employed an eco-friendly method termed green synthesis using *Camellia sinensis* extract and *Prunus africana* extract to produce AgNPs. The FTIR results confirm that the organic phytochemicals in the CSE and PAE facilitate bio-reduction of Ag^+ ion to Ag^o. UV-vis and FESEM analyses revealed that the rate of green synthesis and size distribution of nanoparticles increases with an increase in plant extract concentration and time. PAE- and CSE-biosynthesized AgNPs with different physicochemical properties such as size distribution, degree of agglomeration, charge, and polydispersity; thus, nanoparticle properties are also influenced by the plant species. The CSE- and PAE-photosynthesized AgNPs exhibited potent antibacterial activity against CR clinical isolates at every concentration comparable to the nontoxic dose. The potent antimicrobial activity may be attributed to the small-sized highly penetrative green-synthesized AgNPs and electrostatic interaction between the positively charged AgNPs and the negatively charged bacterial cell membrane. In light of the above, we affirm that the biosynthesized AgNPs are potential future therapeutic agents for treatments of resistant bacterial infections.

DATA AVAILABILITY STATEMENT

The raw data supporting the conclusion of this article will be made available by the authors, without undue reservation.

AUTHOR CONTRIBUTIONS

This work was carried out in collaboration between all authors. JK, MM, JN, DB, and FE conceptualized this project. KS, EW, CK, and JS performed all the laboratory experiments. KS, JK, JS, and MM analyzed the data. KS, EW, JS, and CK wrote the first draft of the manuscript and managed manuscript revisions. All authors read and approved the final manuscript.

FUNDING

ACKNOWLEDGMENTS

SUPPLEMENTARY MATERIAL

The Supplementary Material for this article can be found online at: https://www.frontiersin.org/articles/10.3389/fnano.2021.697303/full#supplementary-material

REFERENCES

Agnihotri, S., Mukherji, S., and Mukherji, S. (2013). Immobilized Silver Nanoparticles Enhance Contact Killing and Show Highest Efficacy: Elucidation of the Mechanism of Bactericidal Action of Silver. *Nanoscale* 5 (16), 7328–7340. doi:10.1039/c3nr00024a

Ajitha, B., Ashok Kumar Reddy, Y., and Sreedhara Reddy, P. (2015). Green Synthesis and Characterization of Silver Nanoparticles Using Lantana Camara Leaf Extract. *Mater. Sci. Eng. C* 49, 373–381. doi:10.1016/j.msec.2015.01.035

Akintelu, S. A., Bo, Y., and Folorunso, A. S. (2020). A Review on Synthesis, Optimization, Mechanism, Characterization, and Antibacterial Application of Silver Nanoparticles Synthesized from Plants. *J. Chem.* 2020, 3189043. doi:10.1155/2020/3189043

Albrecht, M. A., Evans, C. W., and Raston, C. L. (2006). Green Chemistry and the Health Implications of Nanoparticles. *Green. Chem.* 8 (5), 417–432. doi:10.1039/b517131h

Anandalakshmi, K., Venugobal, J., and Ramasamy, V. (2016). Characterization of Silver Nanoparticles by green Synthesis Method Using Pedalium Murex Leaf Extract and Their Antibacterial Activity. *Appl. Nanosci.* 6 (3), 399–408. doi:10.1007/s13204-015-0449-z

Bin Sayeed, M., Karim, S., Sharmin, T., and Morshed, M. (2016). Critical Analysis on Characterization, Systemic Effect, and Therapeutic Potential of Beta-Sitosterol: a Plant-Derived Orphan Phytosterol. *Medicines* 3 (4), 29. doi:10.3390/medicines3040029

Bondarenko, O., Juganson, K., Ivask, A., Kasemets, K., Mortimer, M., and Kahru, A. (2013). Toxicity of Ag, CuO and ZnO Nanoparticles to Selected Environmentally Relevant Test Organisms and Mammalian Cells *In Vitro*: a Critical Review. *Arch. Toxicol.* 87 (7), 1181–1200. doi:10.1007/s00204-013-1079-4

Botten, D., Fugallo, G., Fraternali, F., and Molteni, C. (2015). Structural Properties of Green Tea Catechins. *J. Phys. Chem. B* 119 (40), 12860–12867. doi:10.1021/acs.jpcb.5b08737

Carbin, B.-E., Larsson, B., and Lindahl, O. (1990). Treatment of Benign Prostatic Hyperplasia with Phytosterols. *Br. J. Urol.* 66 (6), 639–641. doi:10.1111/j.1464-410x.1990.tb07199.x

Castillo-Henríquez, L., Alfaro-Aguilar, K., Ugalde-Álvarez, J., Vega-Fernández, L., Montes de Oca-Vásquez, G., and Vega-Baudrit, J. R. (2020). Green Synthesis of Gold and Silver Nanoparticles from Plant Extracts and Their Possible Applications as Antimicrobial Agents in the Agricultural Area. *Nanomaterials* 10 (9), 1763. doi:10.3390/nano10091763

Castro, L., Blázquez, M. L., Muñoz, J. á., González, F. G., and Ballester, A. (2014). Mechanism and Applications of Metal Nanoparticles Prepared by Bio-Mediated Process. *Rev. Adv. Sci. Engng* 3 (3), 199–216. doi:10.1166/rase.2014.1064

CDC (2013). *Antibiotic Resistance Threats in the United States.* U. S. Department of Health and Human Services, Centers for Disease Control and Prevention.

Chattopadhyay, S., Dash, S. K., and Ghosh, T. (2010). Surface modification of cobalt oxide nanoparticles using phosphonomethyl iminodiacetic acid followed by folic acid: a biocompatible vehicle for targeted anticancer drug delivery. *Cancer Nano.* 4, 103–116. doi:10.1007/s12645-013-0042-7

Das, R., Nath, S. S., Chakdar, D., Gope, G., and Bhattacharjee, R. (2010). Synthesis of Silver Nanoparticles and Their Optical Properties. *J. Exp. Nanoscience* 5 (4), 357–362. doi:10.1080/17458080903583915

Dickson, J. S., and Koohmaraie, M. (1989). Cell Surface Charge Characteristics and Their Relationship to Bacterial Attachment to Meat Surfaces. *Appl. Environ. Microbiol.* 55 (4), 832–836. doi:10.1128/aem.55.4.832-836.1989

Durán, N., Nakazato, G., and Seabra, A. (2016). Antimicrobial Activity of Biogenic Silver Nanoparticles, and Silver Chloride Nanoparticles: an Overview and Comments. *J Appl. Microbiol. Biotechnol.* 100 (15), 6555–6570. doi:10.1007/s00253-016-7657-7

ECDC (2018). "European Centre for Disease Prevention and Control; Antimicrobial Resistance Surveillance in Europe 2017," in *Annual Report of the European Antimicrobial Resistance Surveillance Network (EARS-Net)* (Stockholm: ECDC). doi:10.2900/797061

Eram, R., Kumari, P., Panda, P. K., Singh, S., Sarkar, B., Mallick, M. A., et al. (2021). Cellular Investigations on Mechanistic Biocompatibility of Green Synthesized Calcium Oxide Nanoparticles with *Danio rerio*. *J. Nanotheronastics.* 2 (1), 51–62. doi:10.3390/jnt2010004

Forester, S. C., and Lambert, J. D. (2011). The Role of Antioxidant versus Pro-oxidant Effects of green tea Polyphenols in Cancer Prevention. *Mol. Nutr. Food Res.* 55 (6), 844–854. doi:10.1002/mnfr.201000641

Fox, C. L., and Modak, S. M. (1974). Mechanism of Silver Sulfadiazine Action on Burn Wound Infections. *Antimicrob. Agents Chemother.* 5 (6), 582–588. doi:10.1128/aac.5.6.582

Ghante, M. H., and Jamkhande, P. G. (2019). Role of Pentacyclic Triterpenoids in Chemoprevention and Anticancer Treatment: An Overview on Targets and Underling Mechanisms. *J. Pharmacopuncture* 22 (2), 55–67. doi:10.3831/KPI.201.22.007

Gholami, M., Shahzamani, K., Marzban, A., and Lashgarian, H. E. (2018). Evaluation of Antimicrobial Activity of Synthesised Silver Nanoparticles Using Thymus Kotschyanus Aqueous Extract. *IET nanobiotechnol.* 12 (8), 1114–1117. doi:10.1049/iet-nbt.2018.5110

Gong, P., Li, H., He, X., Wang, K., Hu, J., Tan, W., et al. (2007). Preparation and Antibacterial Activity of Fe3O4@Ag Nanoparticles. *Nanotechnology* 18 (28), 285604. doi:10.1088/0957-4484/18/28/285604

Guzmán, M. G., Dille, J., and Godet, S. (2009). Synthesis of Silver Nanoparticles by Chemical Reduction Method and Their Antibacterial Activity. *Int. J. Chem. Biomol. Eng.* 2 (3), 104–111.

Hajiaghaalipour, F., Sanusi, J., and Kanthimathi, M. S. (2016). Temperature and Time of Steeping Affect the Antioxidant Properties of white, green, and Black tea Infusions. *J. Food Sci.* 81 (1), H246–H254. doi:10.1111/1750-3841.13149

Hamouda, R. A., Hussein, M. H., Abo-emlagd, R. A., and Bawazir, S. S. (2019). Synthesis and Biological Characterization of Silver Nanoparticles Derived from the Cyanobacterium Oscillatoria Limnetica. *Sci. Rep.* 9 (1), 13071. doi:10.1038/s41598-019-49444-y

Husain, S., Verma, S. K., Hemlata, fnm., Azam, M., Sardar, M., Haq, Q. M. R., et al. (2021). Antibacterial Efficacy of Facile Cyanobacterial Silver Nanoparticles Inferred by Antioxidant Mechanism. *Mater. Sci. Eng. C* 122, 111888. doi:10.1016/j.msec.2021.111888

Husain, S., Verma, S. K., Yasin, D., Hemlata, F., A. Rizvi, M. M., and Fatma, T. (2021). Facile green Bio-Fabricated Silver Nanoparticles from Microchaete Infer Dose-dependent Antioxidant and Anti-proliferative Activity to Mediate Cellular Apoptosis. *Bioorg. Chem.* 107, 104535. doi:10.1016/j.bioorg.2020.104535

Jafari, A., Jafari Nodooshan, S., Safarkar, R., Movahedzadeh, F., Mosavari, N., Novin Kashani, et al. (2018). Toxicity Effects of AgZnO Nanoparticles and Rifampicin on *Mycobacterium tuberculosis* into the Macrophage. *J. Basic Microbiol.* 58 (1), 41–51. doi:10.1002/jobm.201700289

Jameel, M. S., Aziz, A. A., and Dheyab, M. A. (2020). Green Synthesis: Proposed Mechanism and Factors Influencing the Synthesis of Platinum Nanoparticles %. *J. Green. Process. Synth.* 9 (1), 386–398. doi:10.1515/gps-2020-0041

Kagithoju, S., Godishala, V., and Nanna, R. S. (2015). Eco-friendly and green Synthesis of Silver Nanoparticles Using Leaf Extract of Strychnos Potatorum Linn.F. And Their Bactericidal Activities. *3 Biotech.* 5 (5), 709–714. doi:10.1007/s13205-014-0272-3

Kampa, M., Alexaki, V.-I., Notas, G., Nifli, A.-P., Nistikaki, A., Hatzoglou, A., et al. (2004). Antiproliferative and Apoptotic Effects of Selective Phenolic Acids on T47D Human Breast Cancer Cells: Potential Mechanisms of Action. *Breast Cancer Res.* 6 (2), R63. doi:10.1186/bcr752

Kawata, K., Osawa, M., and Okabe, S. (2009). *In Vitro* toxicity of Silver Nanoparticles at Noncytotoxic Doses to HepG2 Human Hepatoma Cells. *Environ. Sci. Technol.* 43 (15), 6046–6051. doi:10.1021/es900754q

Kayange, N., Kamugisha, E., Mwizamholya, D. L., Jeremiah, S., and Mshana, S. E. (2010). Predictors of Positive Blood Culture and Deaths Among Neonates with Suspected Neonatal Sepsis in a Tertiary Hospital. *Mwanza-Tanzania* 10 (1), 39. doi:10.1186/1471-2431-10-39

Kelly, K. L., Coronado, E., Zhao, L., and Schatz, G. C. (2003). The Optical Properties of Metal Nanoparticles: The Influence of Size, Shape, and Dielectric Environment. *J. Phys. Chem. B* 107 (3), 668–677. doi:10.1021/jp026731y

Kikuzaki, H., Hisamoto, M., Hirose, K., Akiyama, K., and Taniguchi, H. (2002). Antioxidant Properties of Ferulic Acid and its Related Compounds. *J. Agric. Food Chem.* 50 (7), 2161–2168. doi:10.1021/jf011348w

Kumari, P., Panda, P. K., Patel, P., Jha, E., Mallick, M. A., Suar, M., et al. (2020). Biocompatible Biogenic Silver Nanoparticles Interact with Caspases on an Atomic Level to Elicit Apoptosis. *Nanomedicine* 15 (22), 2119–2132.

Kvítek, L., Panáček, A., Soukupová, J., Kolář, M., Večeřová, R., Prucek, R., et al. (2008). Effect of Surfactants and Polymers on Stability and Antibacterial Activity of Silver Nanoparticles (NPs). *J. Phys. Chem. C* 112 (15), 5825–5834. doi:10.1021/jp711616v

Laxminarayan, R., Boeckel, T. V., and Teillant, A. (2015). *The Economic Costs of Withdrawing Antimicrobial Growth Promoters from the Livestock Sector*. OECD Food, Agriculture and Fisheries Papers, No. 78, OECD Publishing. doi:10.1787/5js64kst5wvl-en

Lee, K.-S., and El-Sayed, M. A. (2006). Gold and Silver Nanoparticles in Sensing and Imaging: Sensitivity of Plasmon Response to Size, Shape, and Metal Composition. *J. Phys. Chem. B* 110 (39), 19220–19225. doi:10.1021/jp062536y

Li, W.-R., Xie, X.-B., Shi, Q.-S., Zeng, H.-Y., Ou-Yang, Y.-S., and Chen, Y.-B. (2010). Antibacterial Activity and Mechanism of Silver Nanoparticles on *Escherichia coli*. *Appl. Microbiol. Biotechnol.* 85 (4), 1115–1122. doi:10.1007/s00253-009-2159-5

Livermore, D. M., Warner, M., Mushtaq, S., Doumith, M., Zhang, J., and Woodford, N. (2011). What Remains against Carbapenem-Resistant Enterobacteriaceae? Evaluation of Chloramphenicol, Ciprofloxacin, Colistin, Fosfomycin, Minocycline, Nitrofurantoin, Temocillin and Tigecycline. *Int. J. Antimicrob. Agents* 37 (5), 415–419. doi:10.1016/j.ijantimicag.2011.01.012

Loo, Y. Y., Rukayadi, Y., Nor-Khaizura, M-A-R., Kuan, C. H., Chieng, B. W., Nishibuchi, M., et al. (2018). Vitro Antimicrobial Activity of Green Synthesized Silver Nanoparticles against Selected Gram-Negative Foodborne Pathogens. *Front. Microbiol.*, 9, 1555. doi:10.3389/fmicb.2018.01555

Lu, Z., Rong, K., Li, J., Yang, H., and Chen, R. (2013). Size-dependent Antibacterial Activities of Silver Nanoparticles against Oral Anaerobic Pathogenic Bacteria. *J. Mater. Sci. Mater. Med.* 24 (6), 1465–1471. doi:10.1007/s10856-013-4894-5

Machhi, J., Shahjin, F., Das, S., Patel, M., Abdelmoaty, M. M., Cohen, J. D., et al. (2021). Nanocarrier Vaccines for SARS-CoV-2. *Adv. Drug Deliv. Rev.* 171, 215–239. doi:10.1016/j.addr.2021.01.002

Marková, Z., Šišková, K., Filip, J., Šafářová, K., Prucek, R., Panáček, A., et al. (2012). Chitosan-based Synthesis of Magnetically-Driven Nanocomposites with Biogenic Magnetite Core, Controlled Silver Size, and High Antimicrobial Activity. *Green. Chem.* 14 (9), 2550–2558. doi:10.1039/c2gc35545k

Martinez-Gutierrez, F., Boegli, L., Agostinho, A., Sánchez, E. M., Bach, H., Ruiz, F., et al. (2013). Anti-biofilm Activity of Silver Nanoparticles against Different Microorganisms. *Biofouling* 29 (6), 651–660. doi:10.1080/08927014.2013.794225

McKenzie, C. (2011). Antibiotic Dosing in Critical Illness. *J. Antimicrob. Chemother.* 66 (Suppl. l_2), ii25–ii31. doi:10.1093/jac/dkq516

Mie, R., Samsudin, M. W., Din, L. B., Ahmad, A., Ibrahim, N., and Adnan, S. N. (2014). Synthesis of Silver Nanoparticles with Antibacterial Activity Using the Lichen Parmotrema Praesorediosum. *Int. J. Nanomedicine* 9, 121–127. doi:10.2147/IJN.S52306

Mohamed, H. E. A., Afridi, S., Khalil, A. T., Zia, D., Iqbal, J., Ullah, I., et al. (2019). Biosynthesis of Silver Nanoparticles from Hyphaene Thebaica Fruits and Their *In Vitro* Pharmacognostic Potential. *Mater. Res. Express* 6 (10), 1050c9. doi:10.1088/2053-1591/ab4217

Morones, J. R., Elechiguerra, J. L., Camacho, A., Holt, K., Kouri, J. B., Ramírez, J. T., et al. (2005). The Bactericidal Effect of Silver Nanoparticles. *Nanotechnology* 16 (10), 2346–2353. doi:10.1088/0957-4484/16/10/059

Moyer, C. A., Brentano, L., Gravens, D. L., Margraf, H. W., and Monafo, W. W. (1965). Treatment of Large Human Burns With 0.5 Percent Silver Nitrate Solution. *Arch. Surg.* 90 (6), 812–867. doi:10.1001/archsurg.1965.01320120014002

Nanomedicine and the COVID-19 Vaccines. *Nat. Nanotechnol*, (2020). 15(12): p. 963. doi:10.1038/s41565-020-00820-0

Nasrollahzadeh, M., Sajadi, S. M., and Khalaj, M. (2014). Green Synthesis of Copper Nanoparticles Using Aqueous Extract of the Leaves of Euphorbia esula L and Their Catalytic Activity for Ligand-free Ullmann-Coupling Reaction and Reduction of 4-nitrophenol. *RSC Adv.* 4 (88), 47313–47318. doi:10.1039/c4ra08863h

Nenadis, N., Zhang, H.-Y., and Tsimidou, M. Z. (2003). Structure−Antioxidant Activity Relationship of Ferulic Acid Derivatives: Effect of Carbon Side Chain Characteristic Groups. *J. Agric. Food Chem.* 51 (7), 1874–1879. doi:10.1021/jf0261452

Njagi, E. C., Huang, H., Stafford, L., Genuino, H., Galindo, H. M., Collins, J. B., et al. (2011). Biosynthesis of Iron and Silver Nanoparticles at Room Temperature Using Aqueous Sorghum Bran Extracts. *Langmuir* 27 (1), 264–271. doi:10.1021/la103190n

Pakyz, A. L., Oinonen, M., and Polk, R. E. (2009). Relationship of Carbapenem Restriction in 22 University Teaching Hospitals to Carbapenem Use and Carbapenem-Resistant *Pseudomonas aeruginosa*. *Antimicrob. Agents Chemother.* 53 (5), 1983–1986. doi:10.1128/aac.01535-08

Panáček, A., Kvítek, L., Prucek, R., Kolář, M., Večeřová, R., Pizúrová, N., et al. (2006). Silver Colloid Nanoparticles: Synthesis, Characterization, and Their Antibacterial Activity. *J. Phys. Chem. B*, 110 (33), 16248–16253. doi:10.1021/jp063826h

Pasrija, D., and Anandharamakrishnan, C. (2015). Techniques for Extraction of green tea Polyphenols: a Review. *Food Bioproc. Technol.* 8 (5), 935–950. doi:10.1007/s11947-015-1479-y

Paul, P., Verma, S., Kumar Panda, P., Jaiswal, S., Sahu, B. R., and Suar, M. (2018). Molecular Insight to Influential Role of Hha-TomB Toxin-Antitoxin System for Antibacterial Activity of Biogenic Silver Nanoparticles. *Artif. Cell Nanomedicine, Biotechnol.* 46 (Suppl. 3), S572–S584. doi:10.1080/21691401.2018.1503598

Pirtarighat, S., Ghannadnia, M., and Baghshahi, S. (2019). Green Synthesis of Silver Nanoparticles Using the Plant Extract of Salvia Spinosa Grown *In Vitro* and Their Antibacterial Activity Assessment. *J. Nanostruct Chem.* 9 (1), 1–9. doi:10.1007/s40097-018-0291-4

Polavarapu, L., and Liz-Marzán, L. M. (2013). Growth and Galvanic Replacement of Silver Nanocubes in Organic media. *Nanoscale* 5 (10), 4355–4361. doi:10.1039/c3nr01244a

Pongpiacha, S. J. J. (2014). FTIR Spectra of Organic Functional Group Compositions in PM2. 5 Collected at Chiang-Mai City, Thailand during the Haze Episode in March 2012. *J. Appl. Sci.* 14 (22), 2967–2977. doi:10.3923/jas.2014.2967.2977

Raman, G., Park, S. J., Sakthivel, N., and Suresh, A. K. (2017). Physico-cultural Parameters during AgNPs Biotransformation with Bactericidal Activity against Human Pathogens. *Enzyme Microb. Techn.* 100, 45–51. doi:10.1016/j.enzmictec.2017.02.002

Reithofer, M. R., Lakshmanan, A., Ping, A. T. K., Chin, J. M., and Hauser, C. A. E. (2014). *In Situ* synthesis of Size-Controlled, Stable Silver Nanoparticles within Ultrashort Peptide Hydrogels and Their Anti-bacterial Properties. *Biomaterials* 35 (26), 7535–7542. doi:10.1016/j.biomaterials.2014.04.102

Rizzello, L., Cingolani, R., and Pompa, P. P. (2013). Nanotechnology Tools for Antibacterial Materials. *Nanomedicine* 8 (5), 807–821. doi:10.2217/nnm.13.63

Roca, A., Quintó, L., Abacassamo, F., Morais, L., Vallès, X., Espasa, M., et al. (2008). Nvasive Haemophilus Influenzae Disease in Children Less than 5 Years of Age in Manhiça, a Rural Area of Southern Mozambique. *Trop. Med. Int. Health*, 13 (6), 818–826. doi:10.1111/j.1365-3156.2008.02061.x

Sahni, G., Panwar, A., and Kaur, B. (2015). Controlled green Synthesis of Silver Nanoparticles by Allium cepa and Musa Acuminata with strong Antimicrobial Activity. *Int. Nano Lett.* 5 (2), 93–100. doi:10.1007/s40089-015-0142-y

Sastry, M., Patil, V., and Sainkar, S. R. (1998). Electrostatically Controlled Diffusion of Carboxylic Acid Derivatized Silver Colloidal Particles in Thermally Evaporated Fatty Amine Films. *J. Phys. Chem. B* 102 (8), 1404–1410. doi:10.1021/jp9719873

Schleich, S., Papaioannou, M., Baniahmad, A., and Matusch, R. (2006). Extracts from Pygeum Africanum and Other Ethnobotanical Species with Antiandrogenic Activity. *Planta Med.* 72 (09), 807–813. doi:10.1055/s-2006-946638

Schoenmaker, L., Witzigmann, D., Kulkarni, J. A., Verbeke, R., Kersten, G., Jiskoot, W., et al. (2021). mRNA-Lipid Nanoparticle COVID-19 Vaccines: Structure and Stability. *Int. J. Pharmaceutics* 601, 120586. doi:10.1016/j.ijpharm.2021.120586

Shaik, M., Khan, M., Kuniyil, M., Al-Warthan, A., Alkhathlan, H., Siddiqui, M., et al. (2018). Plant-extract-assisted green Synthesis of Silver Nanoparticles Using Origanum Vulgare L. Extract and Their Microbicidal Activities. *Sustainability* 10 (4), 913. doi:10.3390/su10040913

Simon-Deckers, A., Loo, S., Mayne-L'hermite, M., Herlin-Boime, N., Menguy, N., Reynaud, C., et al. (2009). Size-, Composition- and Shape-dependent Toxicological Impact of Metal Oxide Nanoparticles and Carbon Nanotubes toward Bacteria. *Environ. Sci. Technol.* 43 (21), 8423–8429. doi:10.1021/es9016975

Singh, J., Dutta, T., Kim, K-H., Rawat, M., Samddar, P., and Kumar, P. (2018). 'Green' Synthesis of Metals and Their Oxide Nanoparticles: Applications for Environmental Remediation. *J. Nanobiotechnology* 16 (1), 84. doi:10.1186/s12951-018-0408-4

Ssekatawa, K., Byarugaba, D. K., Nakavuma, J. L., Kato, C. D., Ejobi, F., Tweyongyere, R., et al. (2021). Carbapenem Resistance Profiles of Pathogenic *Escherichia coli* in Uganda. *Ejbio* 2 (2), 63–73. doi:10.24018/ejbio.2021.2.2.171

Ssekatawa, K., Byarugaba, D. K., Kato, C. D., Ejobi, F., Tweyongyere, R., Lubwama, M., et al. (2020). Nanotechnological Solutions for Controlling Transmission and Emergence of Antimicrobial-Resistant Bacteria, Future Prospects, and Challenges: a Systematic Review. *J. Nanoparticle Res.* 22 (5), 117. doi:10.1007/s11051-020-04817-7

Ssekatawa, K., Byarugaba, D. K., Nakavuma, J. L., Kato, D. C, Ejobi, F., Tweyongyere, R., and Eddie, W. M. (2021). Prevalence of Pathogenic *Klebsiella pneumoniae* Based on PCR Capsular Typing Harbouring Carbapenemases Encoding Genes in Uganda Tertiary Hospitals. *Antimicrob. Resist. Infect. Control.* 10 (1), 57. doi:10.1186/s13756-021-00923-w

Tahir, M. N., Natalio, F., Cambaz, M. A., Panthöfer, M., Branscheid, R., Kolb, U., et al. (2013). Controlled Synthesis of Linear and Branched Au@ZnO Hybrid Nanocrystals and Their Photocatalytic Properties. *Nanoscale* 5 (20), 9944–9949. doi:10.1039/c3nr02817h

Takahashi, T., Nagatoishi, S., Kuroda, D., and Tsumoto, K. (2018). Thermodynamic and Computational Analyses Reveal the Functional Roles of the Galloyl Group of tea Catechins in Molecular Recognition. *PLOS ONE* 13 (10), e0204856. doi:10.1371/journal.pone.0204856

Tomaszewska, E., Soliwoda, K., Kadziola, K., Tkacz-Szczesna, B., Celichowski, G., Cichomski, M., Szmaja, W., et al. (2013). Detection Limits of DLS and UV-Vis Spectroscopy in Characterization of Polydisperse Nanoparticles Colloids. *J. Nanomater.* 2013, 313081. doi:10.1155/2013/313081

Usmani, A., Dash, P. P., and Mishra, A. (2018). Metallic Nanoformulations: Green Synthetic Approach for Advanced Drug Delivery. *Mater. Sci.* 2 (2), 1–4.

Venugopal, K., Rather, H. A., Rajagopal, K., Shanthi, M. P., Sheriff, K., Illiyas, M., et al. (2017). Synthesis of Silver Nanoparticles (Ag NPs) for Anticancer Activities (MCF 7 Breast and A549 Lung Cell Lines) of the Crude Extract of Syzygium Aromaticum. *J. Photochem. Photobiol. B: Biol.* 167, 282–289. doi:10.1016/j.jphotobiol.2016.12.013

Verma, S. K., Jha, E., Panda, P. K., Thirumurugan, A., Patro, S., Parashar, S. K. S., et al. (2018). Molecular Insights to Alkaline Based Bio-Fabrication of Silver Nanoparticles for Inverse Cytotoxicity and Enhanced Antibacterial Activity. *Mater. Sci. Eng. C* 92, 807–818. doi:10.1016/j.msec.2018.07.037

Verma, S. K., Jha, E., Panda, P. K., Thirumurugan, A., and Suar, M. (2019). Biological Effects of green-synthesized Metal Nanoparticles: a Mechanistic View of Antibacterial Activity and Cytotoxicity. *Advanced Nanostructured Materials for Environmental Remediation.* Springer, 145–171. doi:10.1007/978-3-030-04477-0_6

Verma, S. K., Jha, E., Sahoo, B., Panda, P. K., Thirumurugan, A., Parashar, S. K. S., et al. (2017). Mechanistic Insight into the Rapid One-step Facile Biofabrication of Antibacterial Silver Nanoparticles from Bacterial Release and Their Biogenicity and Concentration-dependent *In Vitro* Cytotoxicity to colon Cells. *RSC Adv.* 7 (64), 40034–40045. doi:10.1039/c7ra05943d

Verma, S. K., Nisha, K., Panda, P. K., Patel, P., Kumari, P., Mallick, M. A., et al. (2020). Green Synthesized MgO Nanoparticles Infer Biocompatibility by Reducing *In Vivo* Molecular Nanotoxicity in Embryonic Zebrafish through Arginine Interaction Elicited Apoptosis. *Sci. Total Environ.* 713, 136521. doi:10.1016/j.scitotenv.2020.136521

Wang, L., Hu, C., and Shao, L. (2017). The Antimicrobial Activity of Nanoparticles: Present Situation and Prospects for the Future. *I. J. Nanomed.* 12, 1227–1249. doi:10.2147/ijn.s121956

Yin, I. X., Zhang, J., Zhao, I. S., Mei, M. L., Li, Q., and Chu, C. H. (2020). The Antibacterial Mechanism of Silver Nanoparticles and its Application in Dentistry. *I. J. Nanomed.* 15, 2555–2562. doi:10.2147/ijn.s246764

Yoshida, Y., and Niki, E. (2003). Antioxidant Effects of Phytosterol and its Components. *J. Nutr. Sci. Vitaminol.* 49 (4), 277–280. doi:10.3177/jnsv.49.277

Zhang, D., Ma, X-L., Gu, Y., Huang, H., and Zhang, G-W., (2020). Green Synthesis of Metallic Nanoparticles and Their Potential Applications to Treat Cancer. *Front. Chem.*, 8. doi:10.3389/fchem.2020.00799 CrossRef Full Text